Applied Energy 374 (2024) 124075

Contents lists available at ScienceDirect

Applied Energy

journal homepage: www.elsevier.com/locate/apenergy

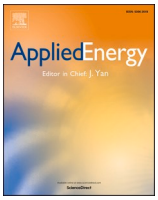

Optimal sitting and sizing of hydrogen refilling stations in distribution networks under locational marginal prices

Marcos Tostado-Véliz [a], Pablo Horrillo-Quintero [b], Pablo García-Triviño [b], Luis M. Fernández-Ramírez [b], Francisco Jurado [a,*]

[a] Department of Electrical Engineering, University of Jaén, 23700 Linares, Spain
[b] Department of Electrical Engineering, ETSI Algeciras, University of Cádiz, Avda. Ramón Puyol, s/n. 11202 Algeciras, Cádiz, Spain

HIGHLIGHTS

- A new tool for sitting and sizing refilling stations in distribution networks is developed.
- Local marginal prices are considered.
- A multi-year iterative algorithm is developed for efficiently solving the problem.
- Local marginal pricing translates nodal electricity costs and helps to allocate assets.
- The installed electrolysis capacity is the most influence parameter in reducing costs.

GRAPHICAL ABSTRACT

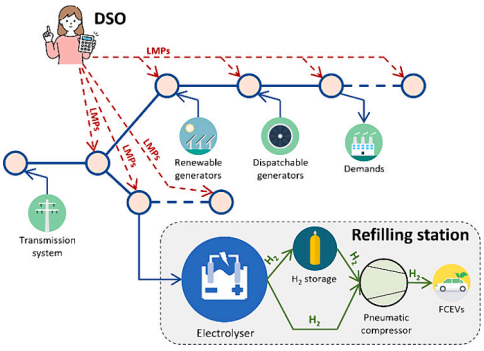

ARTICLE INFO

Keywords:
Electrolysis
Fuel-cell vehicles
Hydrogen storage
Locational marginal pricing

ABSTRACT

The decarbonization of the mobility sector motivates to increase the penetration of battery and fuel-cell electric vehicles. The proliferation of these mobility modes will be accompanied by the massive installation of charging and refilling infrastructures into existing networks. This work focuses on fuel-cell vehicles, for which refilling points are needed. Difficulties in hydrogen transportation can be circumvented by deploying onsite hydrogen generation assets (electrolysers) and storage, which can be partially or fully supplied through local renewable generators. Nevertheless, such assets require a considerable initial investment, being necessary the use of planning tools in order to maximize revenues for private investors. This paper focuses on this issue. In particular, an optimal sitting and sizing tool for hydrogen refilling stations with onsite storage and electrolysers is developed. The developed methodology considers the influence of locational marginal prices, which are cleared by the distribution system operator in order to translate the real electricity cost per node. This pricing strategy helps to best allocate assets through the network and thus resulting valuable for planners in order to site refilling infrastructures properly. An original multi-year iterative algorithm based on the multi-cut Benders' decomposition is proposed in order to alleviate the intrinsic high computational cost of the planning tool while accommodate long-term inflation and degradation rates of parameters. A number of simulations are performed on the well-known IEEE 33-bus system. Results verify that locational marginal pricing effectively translates the nodal

* Corresponding author.
E-mail addresses: mtostado@ujaen.es (M. Tostado-Véliz), pablo.horrillo@uca.es (P. Horrillo-Quintero), pablo.garcia@uca.es (P. García-Triviño), luis.fernandez@uca.es (L.M. Fernández-Ramírez), fjurado@ujaen.es (F. Jurado).

https://doi.org/10.1016/j.apenergy.2024.124075
Received 17 April 2024; Received in revised form 31 May 2024; Accepted 26 July 2024
Available online 1 August 2024

electricity cost to end-users. Remark, the total electrolysis capacity turns out to be the most significant parameter, reducing further the cost of the project, while storage capacity has a limited influence. Results highlight the importance of the infrastructure capacity when determining the placement and sizing of electrolysers, thus supporting decisions when upgrading existing infrastructure. The impact of the number of stations to be installed and the budget cap is also analysed, showing that both parameters have similar influence and may reduce the total project cost by 70% approximately. The typical scheduling behaviour of the electrolysis-storage facilities is discussed, showing how storage is capable to provide energy arbitrage exploiting locational marginal prices. Finally, the computational performance of the developed algorithm is assessed, verifying that the new tool is efficient and portable.

Nomenclature

Acronyms

DG	Distributed generator
DN	Distribution network
DSO	Distribution system operator
FCEV	Fuel-cell electric vehicle
KKT	Karush-Kuhn Tucker
LMP	Locational marginal price
LP	Linear programming
MILP	Mixed-Integer linear programming
PV	Photovoltaic
RES	Renewable energy source
RS	Refilling station

Indices and sets

y	Year $y \in \{1,2,\ldots,Y\}$
s	Scenario $s \in \{1,2,\ldots,S\}$
t	Time $t \in \{1,2,\ldots,T\}$
j,k	Network nodes $j,k \in \{1,2,\ldots,J\}$
$d \in D$	Set of demands
$g \in G^{DG}$	Set of distributed dispatchable generators
$g \in G^{RES}$	Set of non-dispatchable (renewable) generators
$z \in Z$	Set of refuelling stations
Ψ_j/Φ_j	Set of nodes downstream/upstream from the j^{th} node in the network
Ω_j^D	Set of demands connected to the j^{th} node in the network
Ω_j^Z	Set of refilling stations connected to the j^{th} node in the network
Ω_j^G	Set of generators connected to the j^{th} node in the network
κ, ν	Iteration counters

Parameters

r	Inflation/degradation rate (pu)
W	Wholesale electricity price (€/kWh)
ζ^{ex}	Discount rate for exporting electricity (pu)
L	Fuel cost (€/kWh or €/kg)
V^0	Base voltage (volts)
R/X	Branch resistance/inductance (ohm)
$\overline{p}^{sub}/\overline{q}^{sub}$	Maximum active/reactive power at substation (kW/kvar)
$\overline{F}$	Maximum power flow through branches (kVA)
RU/RD	Upward/downward ramping rates of generators (kW)
φ	Reactive portion of generators (pu)
$\widetilde{(\cdot)}$	Indicates a parameter modelled through scenarios
η^Z	Electrolyser efficiency (pu)
LHV_{H_2}	Lower-heating value of hydrogen (kWh/kg)
K^Z/O^Z	Electrolyser capital/maintenance cost (€/kW)
K^H/O^H	Storage tanks capital/maintenance cost (€/kg)
Π	Budget cap (€)
ω_s	Probability of occurrence of scenario s (pu)
M	Large positive constant (−)
N	Maximum number of refuelling stations (−)

Decision variables

p^{im}/p^{ex}	Active power imported/exported at substation (kW)
q^{im}/q^{ex}	Reactive power imported/exported at substation (kvar)
p_g/q_g	Active/reactive power output of the g^{th} generator
p_z	Power consumption (electrolysis) of the z^{th} refilling station (kW)
f^P/f^Q	Active/reactive power flow (kW/kvar)
V	Nodal voltage (volts)
$u^{sub,P}/u^{sub,Q}$	Active/reactive dispatch at substation (binary)
u_g	Commitment of the g^{th} dispatchable generator (binary)
λ	Dual variables linked to equality constraints (€/kWh or €/kg)
$\underline{\mu}/\overline{\mu}$	Dual variables linked to inequality constraints (€/kWh or €/kg)
h_z^{in}/h_z^{out}	Inflow/outflow hydrogen at the z^{th} refilling station (kg)
h_z^d	Hydrogen injected to the demand directly at the z^{th} refilling station (kg)
h_z^{EV}	Hydrogen refilled at the z^{th} refilling station (kg)
H_z	Hydrogen stored at the z^{th} refilling station (kg)
ρ	Slack variable (−)
$\overline{p}_z$	Electrolyser rated power (kW)
$\overline{H}_z$	Hydrogen storage capacity (kg)
δ	Indicates the node where a refuelling station is installed (binary)
γ/ξ	Sensitivities (€/kWh)
β	Auxiliary variable to approach net refilling profit (€)

1. Introduction

Although less remarkably than for other clean mobility technologies, like battery vehicles, sales of fuel-cell electric vehicles (FCEVs) have steadily grown in the last 5 years, especially in some countries like China [1,2]. As seen in Fig. 1, the increment in FCEV sales has been constant (even exponential) in four representative countries, which has not been always accompanied with a proper deployment of refilling infrastructures (see the case of the U.S.). Actually, infrastructure for refilling FCEVs is practically inexistent in most of countries worldwide. For instance, there are barely >10 stations available in Spain currently, most of them managed by private entities [3]. In addition to the clear lack of a proper refilling infrastructure, the penetration of FCEVs is hindered due to the expensive and inefficient hydrogen transportation system [4]. Currently, hydrogen is commonly transported by trucks or existing pipelines, which results costly in most cases.

To overcome such issues and make refilling infrastructures viable, onsite hydrogen generation through mature electrolysis technologies arises as the most feasible alternative, especially when electrolysis is supplied through renewable energy sources (RESs) [5]. Thereby, the

development of proper designing tools for electrolysers and hydrogen tanks devoted on refilling stations (RSs) becomes valuable for private investors, in order to help planners to take decisions in order to maximize the monetary profit of the installation.

Xiao et al. [6] proposed a sizing methodology for standalone RSs with onsite electrolysis and storage. To this end, a simple linear programming (LP) model was developed which neglects important aspects such as degradation or efficiency of electrolyser stacks. Various references employ a software-based methodology for sizing RSs powered by hybrid renewable systems. More specifically, the plant model in [7] includes photovoltaic (PV) and wind generators in combination with stationary battery packs. Likewise, a RS powered by wind energy was optimized in [8], showing that the installation of wind turbines helps to reduce carbon emissions and improve the efficiency of the system notably. The authors in [9] employs the software HOMER to various cases in Turkey and Spain, demonstrating that the combination of different RESs results in the most suitable layout commonly.

Grüger et al. [10] employed evolutionary algorithms to optimally sizing of RSs considering low and high-pressure storage as well as wind turbines. The results obtained show that larger fleets contribute to reduce the cost of hydrogen while considering reserves does not notably increment the cost of the project. Similarly, the authors in [11] considered a swarm-based solver to optimize the operation of a hybrid power plant supplying a charging station for both battery and FCEVs, showing up the proposed methodology is capable to improve the quality of service significantly. The reference [12] also focuses on the optimal operation of refilling infrastructures. In this case, the authors developed an energy management model for microgrids incorporating RSs while considering the interaction with external agents.

In [13], a Mixed-Integer-Linear Programming (MILP) model was proposed for optimal network expansion considering the influence of FCEVs. In this case, the authors assumed the point of view of the distribution system operator (DSO) as particular investor. Dadkhah et al. [14] consider the participation of RSs in day-ahead and balancing markets. In this case, the authors assume the role of a private investor for which a nonlinear model was proposed for optimal sizing the components in the RS. In [15], a risk-constrained optimal operation tool for distribution network (DN) in the presence of FCEVs was proposed. In this case, inherent generation and demand uncertainties are modelled via scenarios, while the level of risk is kept under control and parameterized externally.

Tabandeh et al. [16] proposed a MILP model for optimal network expansion in the presence of RSs. Particularly, this work focuses on partitioning the network into zones which are handled separately. The optimization model casts as a multi-objective framework involving economic and environmental objectives. A day-ahead operation tool for RSs was presented in [17], considering different uncertainty models to take into account the risk associated to renewable generation, prices and FCEV demand. In this sense, a hybrid stochastic-robust methodology was developed, in which the hydrogen demand is modelled using a suited methodology considering particular behaviour and features of FCEVs. Abdelghany et al. [18] develop a model predictive control for a hydrogen storage system locally powered by a wind farm and devoted on supplying FCEVs. To this end, a multi-level scheduling strategy is proposed, capable of handling different variables over different time horizons efficiently.

Dong et al. [19] proposed an integrated network expansion model for hybrid hydrogen-electricity networks. In this case, the nonconvexities arisen from modelling both networks are handled using different linearization tricks based on piecewise approximations, resulting finally in a tractable MILP model. Similarly, the authors of [20] developed a MILP framework for optimal network expansion considering different hydrogen chains (trucks and pipelines). One of the merits of this work lies in the fact of considering quality of service indicators regarding waiting time of FCEVs, whose impact is thus implicitly included in the planning process. A simulated-based tool was developed in [21] for optimizing the operation of onsite hydrogen RSs, reaching out a compromise between satisfaction of users, economy and emissions.

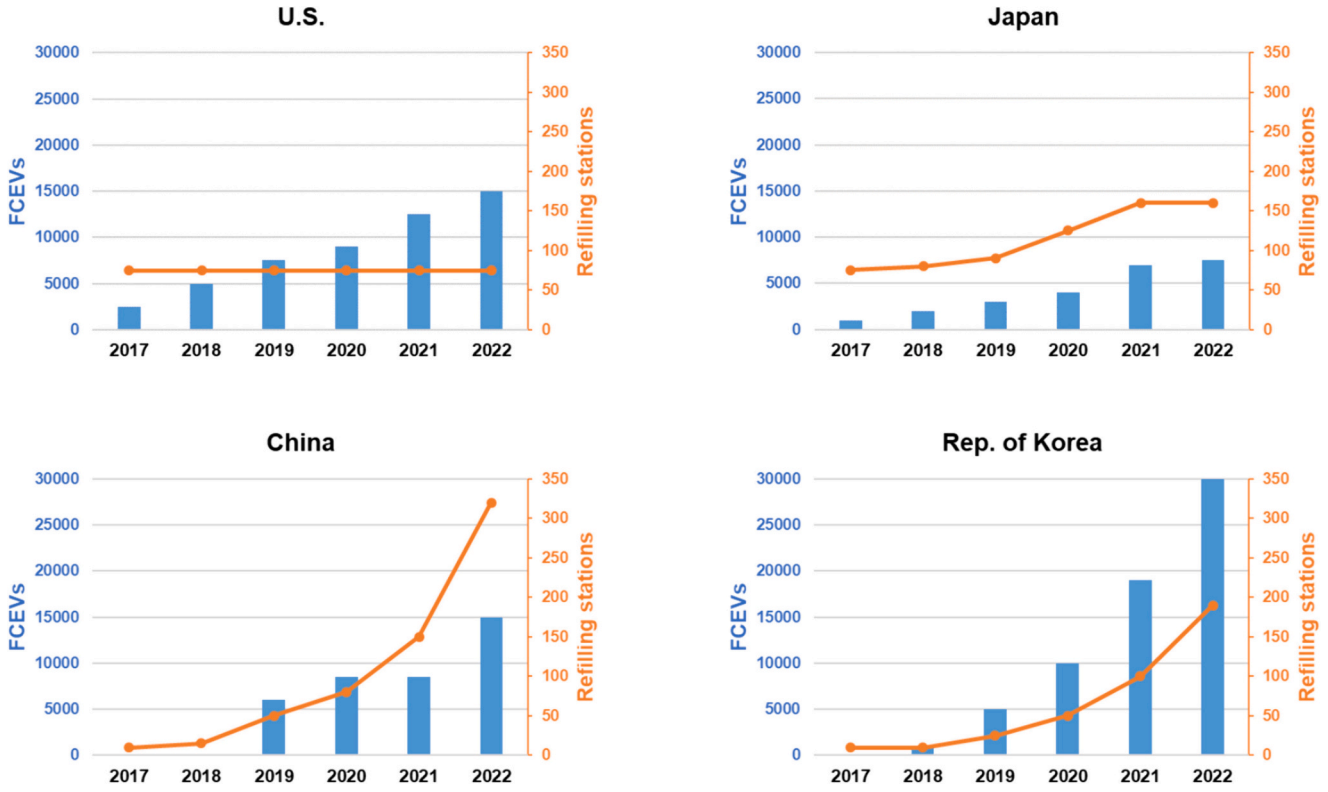

Fig. 1. Development trends for FCEV deployment and refilling infrastructure in the four countries with the highest number of FCEV on the road at the end of 2022 [2].

This work motivates in various gaps encountered in the literature which are, for simplicity, summarized in Table 1. For easing the analysis, we discarded those references devoted on operation stages as this work focuses on planning stages of RSs. In this regard, it is worth differentiating two types of problem. On the one hand, sizing methodologies optimize the rated power or storage capacity of RSs. These methodologies are typically conceived from the point of view of private investors who aim at maximizing their own profit through refilling vehicles. On the other hand, network expansion tools are rather focused on installing new lines or generators integrated into existing networks due to the emergence of FCEVs, which may put on the limit existing infrastructures. In contrast, network expansion problems are typically performed from the point of view of the DSO, who is responsible of carrying investments in order to provide a minimum quality of service.

Nevertheless, such references present two drawbacks which aim to be addressed in this work. Firstly, existing planning methodologies are no longer valid for deregulated networks, where the electricity price is different at each node being determined according to internal market rules [22]. This practice, known as locational marginal pricing, seeks for sending valid market signals in order to guide investors to best allocate assets through the network, as well as leverage intrinsic flexibility of local consumers. This kind of local market mechanisms has been applied to RSs in [23,24]. However, these references focus on operation stages and therefore there is a lack of a proper planning tool to allocate RSs in deregulated DNs, in line with the methodology developed in [22] for stationary batteries.

On the other hand, methodologies proposed for optimal sizing RSs or network expansion in the presence of FCEVs devise as direct solution strategies, without proposing alternatives to handle large databases. Note that this point is critical in designing stages, when planners typically deal with a considerable amount of data regarding electricity prices, demand or renewable potential. Thereby, existing planning methodologies may fail if the amount of data is especially large, resulting in heavy optimization frameworks unaffordable for average machines and solvers. Moreover, important aspects in planning tools such as long-term variation of parameters (e.g. degradation of components) may be difficult to include in existing direct solution methodologies.

Table 1
A summary of the relevant literature.

Refs.	Problem	Features	Solution
[6–9], [14]	Sizing	Typically conceived for private investors who seek for maximizing their own profit selling hydrogen to vehicles. These problems look for sizing components such as renewable generators, electrolysers or storage, typically	Direct
[13,16,19,20]	Network expansion	Typical problem performed by the DSO of other utilities looking for optimally upgrade network assets such as lines, transformers or generators, typically	
[23,24]	Operation with locational marginal pricing	Locational marginal prices are derived somehow in order to send local market signals to each node individually	
This paper	Sizing and sitting with locational marginal pricing	In line with [21], seeks for optimally sitting and sizing RSs in the presence of locational marginal prices, which helps to take better planning decisions	Decomposition

To overcome the shortcomings mentioned above, the objectives of this work are threefold:

- Developing an optimal sizing and sitting methodology for RSs partaking in deregulated DNs. This way, locational marginal prices (LMPs) are incorporated into the optimization process in an original iterative way, allowing investors to best allocate their assets based on local market signals.
- Proposing a solution strategy based on the Benders' decomposition method [25], in order to manage large datasets efficiently. In this sense, we consider a data-driven methodology assuming that local measures of relevant parameters are available at the beginning of the planning horizon.
- Unlike to typical decomposition frameworks, we propose a multi-year multi-scenario strategy which allows to model long-term degradation/inflation of parameters easily. Moreover, the proposed methodology naturally results in a multi-cut Benders' strategy [26], which speeds up the iterative algorithm and thus obtaining valid solutions more rapidly.

In the rest of this paper, Section 2 describes the problem, assumptions and input data, as well as explaining the basic notations of the mathematical modelling. Section 3 introduces the mathematical models of the network and RS. Section 4 develops the solution strategy based on the Benders' decomposition method. Section 5 focuses on validating the new proposal proving a variety of results with analysis. Finally, the paper is concluded with Section 6.

2. Preliminaries

2.1. Problem statement

We focus on a DN including local demand, dispatchable (microturbines) and renewable distributed generators (DGs), as sketched in Fig. 2. The network and assets involved are scheduled daily by the DSO, who is responsible on deciding the power dispatch of each generator in order to minimize the cost of operating the network.

The DN is connected to an upscale transmission system at a unique node, in which the price is cleared at the wholesale electricity market. In contrast, the DSO launches hourly local markets in order to determine LMPs at each node of the network, under which generators and loads are paid/pay for electricity generation and supply, respectively.

This paper focuses on optimal sitting and sizing RSs in the considered DN. The RS is assumed to incorporate local hydrogen generation through electrolysers. This paper does not assume a particular electrolysis technology, but it is worth mentioning that alkaline and polymer membrane electrolysers are the most common technologies nowadays [27]. The station incorporates onsite storage by means of gaseous vessels, while the demand can be satisfied directly from the electrolyser or stored to be supplied later, thus enabling energy arbitrage. Before being supplied to FCEVs, the hydrogen needs to be pressurized to 350 or 700 bar. In this work, we assume the use of pneumatic compressors, which are safer than electrical ones [28].

2.2. Characterization of input data

We propose a data-driven approach assuming that data regarding local demand (electricity and hydrogen), renewable potential and wholesale electricity markets are available for a reasonable period of time (e.g. 1 year). The proposed methodology considers scheduling of assets within periods of one hour which would result in a considerable amount of data. In practice, managing such large datasets in optimization problems is challenging and may suppose intractability issues in conventional machines and solvers.

To overcome the issues above, we consider a characterization of the

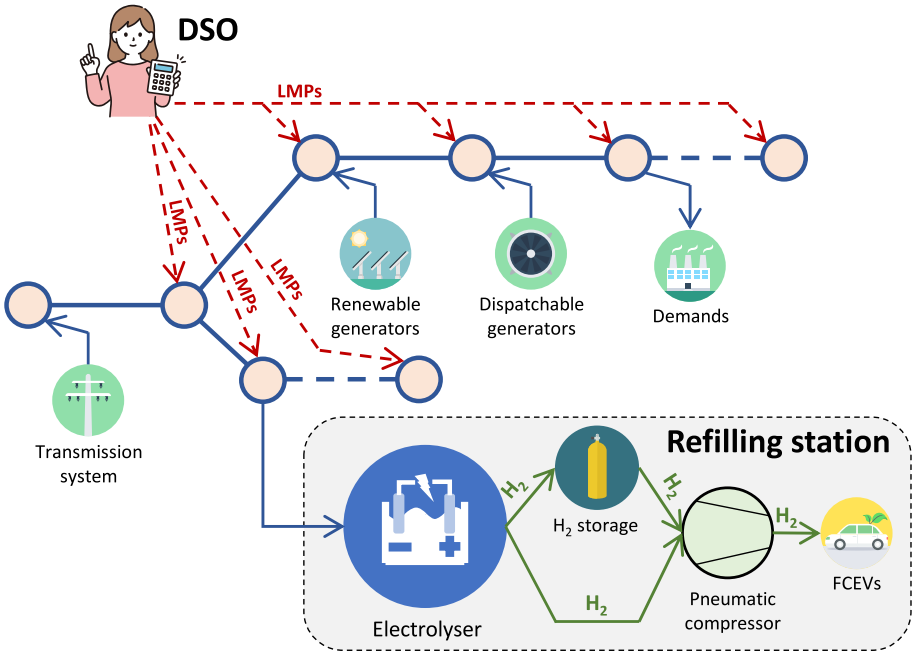

Fig. 2. Sketch of the considered DN wherein the RS will be installed.

input data by means of three representative scenarios namely average, optimistic and pessimistic. The optimistic and pessimistic cases make mention to extreme scenarios of input profiles according their expected impact on final results. For example, it is clear that assuming high renewable potential together with low wholesale prices will affect favourably in the final project results. On the other hand, the average profile corresponds to the most probable input in the original dataset.

To construct these three profiles, we firstly run the k-medoids algorithm taking only one cluster (see [29] for details), taking the result as the average profile. Note that by default, the k-medoids will select those data that characterize best the whole dataset and therefore it seems reasonable considering it as the average profile. The other profiles are taking as the highest and lowest average values within the considered databases. For the sake of simplicity, Table 2 reports the assumptions made on the different input data in order to build the scenarios.

Note that this data characterization based on three scenarios aligns with the methodology proposed in [30]. However, such reference considers equi-probable scenarios, which is not reasonable as extreme cases are expected to have much lower probabilities compared to the average profile. Instead, we calculate joint probabilities for input profiles following the methodology described in [22].

2.3. Notations and assumptions

We assume a project horizon of Y years, each one represented by three scenarios included in the set S. Each scenario represents a day-ahead scheduling plan divided into $T = 24$ time slots. The DN is formed by J nodes and includes dispatchable and renewable generators, gathered in the sets G^{DG} and G^{RES}, respectively; while D stands for the set of demands. For simplicity, we assume that demands are inflexible and only some buses through the network are feasible locations for installing RSs, which are included in the set Z.

We propose in this paper a tool capable of deciding the optimal sitting and sizing for $N \leq Z$ RSs, so that the main results obtained are the rated power of electrolysis stage (i.e. $\overline{p}^{Z}$) as well as the total storage capacity (i.e. $\overline{H}$), together with the most suitable bus/es $z \in Z$ for the installation. In this way, we adopt a power-based electrolyser modelling, which is suitable for this kind of problems and aligns with the decisions taken by the DSO (i.e. power dispatch).

Table 2
Assumptions to build optimistic and pessimistic scenarios.

Data	Optimistic	Pessimistic
Local electricity demand	Low	High
FCEV demand	High	Low
Wholesale electricity price	Low	High
Renewable potential	High	Low

2.4. Long-term degradation/inflation of parameters

Some input parameters vary throughout the project lifetime. For instance, degradation of PV panels provokes a loss in their generation capacity [31]. Such degradation may cause a major impact on final results and therefore should be assumed in the planning project. The multi-year approach considered in this paper allows introducing long-term degradation/inflation of parameters easily. Let us consider a parameter σ with degradation/inflation rate $r \geq 0$, its value at the y^{th} year can be calculated as

$$\sigma_y = \sigma_1(1 \pm r(y-1)); \forall y \in Y \quad (1)$$

Note that (1) is valid for degradation and inflation rates just exchanging the plus/minus sign consequently.

3. Mathematical models

Throughout this section we present the mathematical models corresponding to the optimal planning tool. It is worth noting that dual variables are shown at the right-hand side of each equation.

3.1. Distribution network

The DSO intends to supply the local demand at minimum cost, for which distributed generators are optimally managed through adequate power and commitment signals, leading to the following optimization model between brackets $\langle\cdot\rangle$:

$$\min_{\boldsymbol{x}_{y,s},\boldsymbol{u}_{y,s}} NC_{y,s} = \sum_{t\in T}\left\{\widetilde{W}_{y,s,t}\left(p^{im}_{y,s,t} - \zeta^{ex}p^{ex}_{y,s,t}\right) + \sum_{g\in G^{DG}} L_{y,g}p_{y,g,t}\right\} \tag{2a}$$

Subject to:

$$p^{im}_{y,s,t} - p^{ex}_{y,s,t} = f^{P}_{(j=0),y,s,t}; \forall t \in T \tag{2b}$$

$$q^{im}_{y,s,t} - q^{ex}_{y,s,t} = f^{Q}_{(j=0),y,s,t}; \forall t \in T \tag{2c}$$

$$f^{P}_{j,y,s,t} = \sum_{d\in\Omega^{D}_{j}}\widetilde{p}_{d,y,s,t} + \sum_{z\in\Omega^{Z}_{j}} p_{z,y,s,t} - \sum_{g\in\Omega^{G}_{j}} p_{g,y,s,t} + \sum_{k\in\Psi_{j}} f^{P}_{k,y,s,t}, \left\langle \lambda^{P}_{j,y,s,t}\right\rangle; \forall j \in J\backslash\{0\} \wedge t \in T \tag{2d}$$

$$f^{Q}_{j,y,s,t} = \sum_{d\in\Omega^{D}_{j}}\widetilde{q}_{d,y,s,t} + \sum_{z\in\Omega^{Z}_{j}} q_{z,y,s,t} - \sum_{g\in\Omega^{G}_{j}} q_{g,y,s,t} + \sum_{k\in\Psi_{j}} f^{Q}_{k,y,s,t}; \forall j \in J\backslash\{0\} \wedge t \in T \tag{2e}$$

$$V_{(j=0),y,s,t} = V^{0}; \forall t \in T \tag{2f}$$

$$V_{j,y,s,t} = \sum_{k\in\Phi_{j}} V_{k,y,s,t} - \frac{1}{V^{0}}\left(R_{j}f^{P}_{j,y,s,t} + X_{j}f^{Q}_{j,y,s,t}\right); \forall j \in J\backslash\{0\} \wedge t \in T \tag{2g}$$

$$0 \le p^{im}_{y,s,t} \le u^{sub,P}_{y,s,t}\overline{p}^{sub}; \forall t \in T \tag{2h}$$

$$0 \le p^{ex}_{y,s,t} \le \left(1 - u^{sub,P}_{y,s,t}\right)\overline{p}^{sub}; \forall t \in T \tag{2i}$$

$$0 \le q^{im}_{y,s,t} \le u^{sub,Q}_{y,s,t}\overline{q}^{sub}; \forall t \in T \tag{2j}$$

$$0 \le q^{ex}_{y,s,t} \le \left(1 - u^{sub,Q}_{y,s,t}\right)\overline{q}^{sub}; \forall t \in T \tag{2k}$$

$$\sqrt{\left(f^{P}_{j,y,s,t}\right)^{2} + \left(f^{Q}_{j,y,s,t}\right)^{2}} \le \overline{F}_{j}; \forall j \in J \wedge t \in T \tag{2l}$$

$$0.95V^{0} \le V_{j,y,s,t} \le 1.05V^{0}; \forall j \in J \wedge t \in T \tag{2m}$$

$$u_{g,y,s,t}\underline{p}_{g} \le p_{g,y,s,t} \le u_{g,y,s,t}\overline{p}_{g}; \forall g \in G^{DG} \wedge t \in T \tag{2n}$$

$$-RD_{g} \le p_{g,y,s,t} - p_{g,y,s,(t-1)} \le RU_{g}; \forall g \in G^{DG} \wedge t \in T\backslash\{1\} \tag{2o}$$

$$0 \le p_{g,y,s,t} \le \widetilde{p}_{g,y,s,t}; \forall g \in G^{RES} \wedge t \in T \tag{2p}$$

$$0 \le p_{z,y,s,t} \le \overline{p}_{z}, \left\langle \underline{\mu}_{z,y,s,t}, \overline{\mu}_{z,y,s,t}\right\rangle; \forall z \in Z \wedge t \in T \tag{2q}$$

$$-\overline{p}_{g}\varphi_{g} \le q_{g,y,s,t} \le \overline{p}_{g}\varphi_{g}; \forall g \in G^{DG} \wedge t \in T \tag{2r}$$

$$0 \le q_{g,y,s,t} \le p_{g,y,s,t}\varphi_{g}; \forall g \in G^{RES} \wedge t \in T \tag{2s}$$

$$\boldsymbol{u}_{y,s} \in \{0,1\} \tag{2t}$$

where $\boldsymbol{x}_{y,s} = \left\{p^{im}_{y,s,t}, p^{ex}_{y,s,t}, q^{im}_{y,s,t}, q^{ex}_{y,s,t}, p_{y,g,t}, q_{y,g,t}, p_{z,y,s,t}, f^{P}_{j,y,s,t}, f^{Q}_{j,y,s,t}, V_{j,y,s,t}\right\}$ and $\boldsymbol{u}_{y,s} = \left\{u^{sub,P}_{y,s,t}, u^{sub,Q}_{y,s,t}, u_{g,y,s,t}\right\}$.

The objective function (2a) is composed of two terms. Firstly, the cost of exchanging power with the transmission network under wholesale prices modelled through scenarios. As customary, we consider that exporting pricing is a portion of importing ones $0 \le \zeta^{ex} < 1$ [32], thus reflecting a scenario with surplus generation as frequently in many power systems. Secondly, the fuel cost of dispatchable DGs, assuming that renewable generators have a null marginal cost [33].

In the set of constraints, (2b) and (2c) reflect active and reactive power balances at the root node (substation), respectively. (2d) and (2e) model active and reactive power flows through branches using the well-known LinDistFlow model [34], whose branch modelling is depicted in Fig. 3. Note that this model is suitable for radial distribution networks due to the inclusion of voltage nodal equations, which are neglected in other power flow models [35]. In this regard, the use of the LinDistFlow in radial distribution networks is widely extended and its suitability has been proved in a number of references [36].

The voltage at the root node is fixed in (2f) and commonly taken as the nominal network voltage, whereas (2g) calculates the voltage in the rest of the buses. The set of constraints (2h)-(2k) limit the active and reactive power at substation and, in addition, makes the importing and exporting processes complementary through the inclusion of binary commitment variables. (2l) establishes power limits of branches whereas (2m) limits the nodal voltages within secure bounds. (2n) and (2o) impose upper/lower bounds and ramping limits on dispatchable generators (commonly microturbines or diesel engines), respectively. (2p) limits the output of renewable generators to predicted potentials, which are modelled through scenarios.

The power limit of electrolysers is given in (2q). Note that we include here all the candidate buses disregarding a RS is actually installed or not. This adoption allows a simpler formulation, imposing $\overline{p}_{z} = 0$ at those nodes where electrolysers are not installed. In (2), $\overline{p}_{z}$ is considered a parameter whose value is calculated at other stages as explained later. (2r) and (2s) give reactive power injections from generators. This way, we consider that renewable generators can contribute to reactive power generation through coupling inverters [37]. Finally, binary variables are declared in (2t).

Optimization framework (2) is a Mixed Integer Second Order Programming for which effective off-the-shelf solvers are available [38]. Nevertheless, we propose transforming it into an MILP by linearizing power flow limits (2l), following the approach detailed in the Appendix. On the other hand, it is worth noting that LMPs can be calculated as the sensitivities (dual variables) of (2d). However, sensitivities of MILP problems cannot be derived accurately [39]. In Section 4, we detail a simple methodology to circumvent this issue and calculate LMPs easily.

3.2. Refilling station

In this paper, a simplified electrolyser modelling has been adopted without including binary operational statuses. This adoption is justified in the following assumptions:

- Electrolysers can be modelled using a two-state (on/off) or three-state (on/off/standby) models [40]. Nevertheless, we observed that a well-sized electrolyser is typically operated continuously throughout the day. Under such premise, the operating states can be neglected. Note that this assumption aligns with the conclusions in [41], where it is verified that a simplified electrolyser model is often assumable for planning purposes.
- Neglecting operational states avoids including start-up and shut-down costs. However, by assuming the previous point, on-off

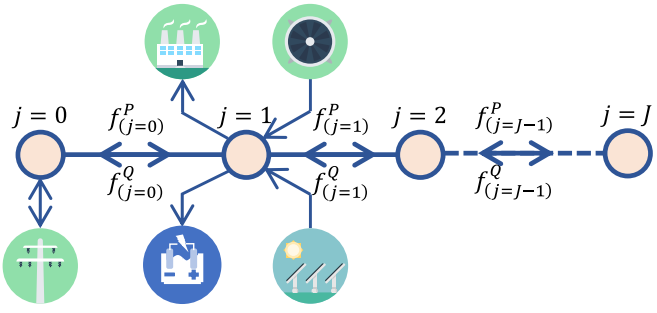

Fig. 3. LinDistFlow branch modelling.

transitions would be infrequent throughout the project lifetime and therefore such costs have a marginal impact on the project.
- Ramping limits can be neglected on the basis of a 1-h dispatchable time step [41].
- A constant efficiency factor can be taken assuming that the electrolyser will work close to its nominal power most of the time.

This way, the electrolyser has been simply modelled imposing an upper bound in (2q). The assumptions above have been verified through multiple experiments, thus confirming their plausibility in the considered planning problem. Below, we present the rest of constraints that, together with (2q), complete the RS model.

$$\frac{p_{z,y,s,t}\eta^{Z}}{\mathrm{LHV}_{\mathrm{H_2}}} = h^{in}_{z,y,s,t} + h^{d}_{z,y,s,t}, \left\langle \lambda^{in}_{z,y,s,t} \right\rangle; \forall z \in Z \wedge t \in T \tag{3a}$$

$$h^{out}_{z,y,s,t} + h^{d}_{z,y,s,t} = h^{EV}_{z,y,s,t}, \left\langle \lambda^{EV}_{z,y,s,t} \right\rangle; \forall z \in Z \wedge t \in T \tag{3b}$$

$$H_{z,y,s,t} = H_{z,y,s,t-1} + h^{in}_{z,y,s,t} - h^{out}_{z,y,s,t}, \left\langle \lambda^{H}_{z,y,s,t} \right\rangle; \forall z \in Z \wedge t \in T \backslash \{1\} \tag{3c}$$

$$H_{z,y,s,(t=1)} = H_{z,y,s,(t=T)} = 0, \left\langle \lambda^{H}_{z,y,s,(t=1)}, \lambda^{H(T)}_{z,y,s} \right\rangle; \forall z \in Z \tag{3d}$$

$$h^{in}_{z,y,s,t}, h^{out}_{z,y,s,t}, h^{d}_{z,y,s,t} \geq 0, \left\langle \underline{\mu}^{in}_{z,y,s,t}, \underline{\mu}^{out}_{z,y,s,t}, \underline{\mu}^{d}_{z,y,s,t} \right\rangle; \forall z \in Z \wedge t \in T \tag{3e}$$

$$0 \leq h^{EV}_{z,y,s,t} \leq \widetilde{h}^{EV}_{z,y,s,t}, \left\langle \underline{\mu}^{EV}_{z,y,s,t}, \overline{\mu}^{EV}_{z,y,s,t} \right\rangle; \forall z \in Z \wedge t \in T \tag{3f}$$

$$0 \leq H_{z,y,s,t} \leq \overline{H}_{z}, \left\langle \underline{\mu}^{H}_{z,y,s,t}, \overline{\mu}^{H}_{z,y,s,t} \right\rangle; \forall z \in Z \wedge t \in T \tag{3g}$$

Above, (3a) states that hydrogen production (as a function of the electrolyser efficiency and lower-heating value of hydrogen) can be directly injected to the FCEVs or stored. (3b) establishes a hydrogen mass balance between the storage output and the demand of FCEVs, which is considered a parameter modelled through scenarios. (3c) indicates the instantaneous state-of-charge (SOC) of the hydrogen tank. (3d) fixes the initial and final hydrogen stored to avoid storage depletion whereas (3e)-(3 g) impose limits on variables.

Note that we do consider null lower bounds for electrolyser power and hydrogen storage in (2q) and (3g), respectively. This assumption contradicts typical operating conditions of electrolysers. For example, minimum operating power of alkaline electrolysers is about 15–20% of its nominal power [41]. However, we adopt here a net-value model assuming that sizing results should be increased accordingly. For example, in case of obtaining a value of $\overline{p}_z = 100$ kW, the real size of the electrolyser should be increased by 20% (120 kW) to reflect real operating conditions. This aspect is taken into account later in the planning model, increasing the capital costs properly.

Including the model (3a)-(3g) in (2) is not advisable since it would lead to the trivial solution $p_z = 0; \forall t \in T$. Indeed, the DSO is not a priori interested on dispatching hydrogen demand due to this agent is not paid for refilling. Note that we consider in this paper that the RS is an independent agent who seeks incrementing her own profit and therefore payments for refilling cannot be included in the objective function of the DSO (2a). To solve these issues, we follow the strategy depicted in Fig. 4, by which the RS is modelled as a virtual agent that can be integrated in (2) through its Karush-Kuhn-Tucker (KKT) conditions. Note that (3a)-(3g) is linear since we considered a simplified electrolyser model, and therefore the KKT conditions are sufficient conditions for optimality [42]. This way, the objective of the RS is implicitly assumed in the DSO model within a Stackelberg game framework (see [43] for details), in which the DSO acts as leader and the RS as follower. Specifically, the KKT conditions for the RS are given below.

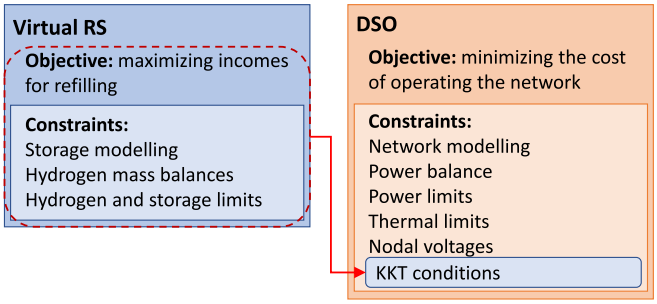

Fig. 4. The proposed virtual RS agent and its interaction with the DSO.

$$\frac{\lambda^{in}_{z,y,s,t}\eta^{Z}}{\mathrm{LHV}_{\mathrm{H_2}}} + \rho_{z,y,s,t} - \underline{\mu}_{z,y,s,t} + \overline{\mu}_{z,y,s,t} = 0; \forall z \in Z \wedge t \in T \tag{3h}$$

$$-\lambda^{in}_{z,y,s,t} - \lambda^{H}_{z,y,s,t} - \underline{\mu}^{in}_{z,y,s,t} = 0; \forall z \in Z \wedge t \in T \tag{3i}$$

$$-\lambda^{in}_{z,y,s,t} + \lambda^{EV}_{z,y,s,t} - \underline{\mu}^{d}_{z,y,s,t} = 0; \forall z \in Z \wedge t \in T \tag{3j}$$

$$\lambda^{EV}_{z,y,s,t} + \lambda^{H}_{z,y,s,t} - \underline{\mu}^{out}_{z,y,s,t} = 0; \forall z \in Z \wedge t \in T \tag{3k}$$

$$-L^{EV}_{y} - \lambda^{EV}_{z,y,s,t} - \underline{\mu}^{EV}_{z,y,s,t} + \overline{\mu}^{EV}_{z,y,s,t} = 0; \forall z \in Z \wedge t \in T \tag{3l}$$

$$\lambda^{H}_{z,y,s,t} - \lambda^{H}_{z,y,s,t+1} - \underline{\mu}^{H}_{z,y,s,t} + \overline{\mu}^{H}_{z,y,s,t} = 0; \forall z \in Z \wedge t \in T \backslash \{T\} \tag{3m}$$

$$\lambda^{H}_{z,y,s,(t=T)} + \lambda^{H(T)}_{z,y,s} - \underline{\mu}^{H}_{z,y,s,(t=T)} + \overline{\mu}^{H}_{z,y,s,(t=T)} = 0; \forall z \in Z \tag{3n}$$

$$0 \leq p_{z,y,s,t} \perp \underline{\mu}_{z,y,s,t} \geq 0; \forall z \in Z \wedge t \in T \tag{3o}$$

$$0 \leq \overline{p}_{z} - p_{z,y,s,t} \perp \overline{\mu}_{z,y,s,t} \geq 0; \forall z \in Z \wedge t \in T \tag{3p}$$

$$0 \leq h^{in}_{z,y,s,t} \perp \underline{\mu}^{in}_{z,y,s,t} \geq 0; \forall z \in Z \wedge t \in T \tag{3q}$$

$$0 \leq h^{d}_{z,y,s,t} \perp \underline{\mu}^{d}_{z,y,s,t} \geq 0; \forall z \in Z \wedge t \in T \tag{3r}$$

$$0 \leq h^{out}_{z,y,s,t} \perp \underline{\mu}^{out}_{z,y,s,t} \geq 0; \forall z \in Z \wedge t \in T \tag{3s}$$

$$0 \leq h^{EV}_{z,y,s,t} \perp \underline{\mu}_{z,y,s,t} \geq 0; \forall z \in Z \wedge t \in T \tag{3t}$$

$$0 \leq \widetilde{h}^{EV}_{z,y,s,t} - h^{EV}_{z,y,s,t} \perp \overline{\mu}^{EV}_{z,y,s,t} \geq 0; \forall z \in Z \wedge t \in T \tag{3u}$$

$$0 \leq H_{z,y,s,t} \perp \underline{\mu}^{H}_{z,y,s,t} \geq 0; \forall z \in Z \wedge t \in T \tag{3v}$$

$$0 \leq \overline{H}_{z} - H_{z,y,s,t} \perp \overline{\mu}^{H}_{z,y,s,t} \geq 0; \forall z \in Z \wedge t \in T \tag{3w}$$

$$\lambda_{y,s} : \text{free} \tag{3x}$$

$$\boldsymbol{\mu}_{y,s} \geq 0 \tag{3y}$$

where $\perp$ stands for complementarity, while $\boldsymbol{\lambda}$ and $\boldsymbol{\mu}$ collect the λ's and the μ's, respectively.

KKT conditions are composed by the stationary conditions (3h)-(3n), the complementarity conditions (3o)-(3w) and the dual feasibility conditions (3x) and (3y). For further details about how to derive the KKT conditions, the reader is referred to [30]. A slack variable ρ is included in (3h) to avoid infeasibility since some limits on p_z have not been included, for simplicity.

Note that complementarity conditions are nonlinear but can be linearized using the well-known big-M method [44], for which the strategy in [45] has been followed to tune the value of big-M's

adequately. After applying this linearization trick, (3) transforms into a tractable MILP.

3.3. Planning framework

The developed planning framework for optimally sizing RSs writes as

$$\min_{\substack{\overline{p}_z,\overline{H}_z,\delta_z,\boldsymbol{x}_{y,s},\boldsymbol{u}_{y,s},\\ \rho_{z,y,s,t},\lambda_{y,s},\mu_{y,s}}} \sum_{z\in Z}\left\{\begin{array}{c} 1.2\overline{p}_z\left(K^Z+\sum_{y\in Y}O_y^Z\right)+1.2\overline{H}_z\left(K^H+\sum_{y\in Y}O_y^H\right)+ \\ \sum_{y\in Y}\sum_{s\in S}\omega_s\sum_{t\in T}\left\{\lambda^P_{z,y,s,t}p_{z,y,s,t}-L_y^{EV}h^{EV}_{z,y,s,t}\right\}\end{array}\right\} \tag{4a}$$

Subject to:

$$1.2K^Z\sum_{z\in Z}\overline{p}_z+1.2K^H\sum_{z\in Z}\overline{H}_z\leq\Pi \tag{4b}$$

$$\overline{p}_z\leq\delta_z M;\forall z\in Z \tag{4c}$$

$$\overline{H}_z\leq\delta_z M;\forall z\in Z \tag{4d}$$

$$\sum_{z\in Z}\delta_z\leq N \tag{4e}$$

$$(2b)-(2t) \tag{4f}$$

$$(3) \tag{4g}$$

The first line in (4a) includes the capital and maintenance costs, which have been increased by 20% in order to assume that the variables $\overline{p}_z$ and $\overline{H}_z$ are actually net values, as discussed before. This way, we assume that the actual sizing values are a 20% higher than the results obtained, thus considering a minimum operating power of 20% and a depth-of-discharge of 80%, common values for this kind of installations [17,41]. On the other hand, the second line in (4a) represents the profit of the RSs, which pay for importing energy under LMPs and are paid for hydrogen refilling. Note that this profit is evaluated under a scenario basis and thus multiplied by the probability of each scenario, thus evaluating it over the entire project horizon. (4b) imposes a budget cap on the capital costs. (4d) and (4e) flag those nodes where the RS is installed, while (4e) limit the number of RSs installed. Finally, (4f) and (4 g) include the DSO and RS models in the framework, respectively.

Framework (4) needs to manage a large amount of data. Note that each variable span for J nodes, Y years, 3 scenarios and 24 time slots. Assuming average conditions, each variable would gather a total of 35,640 elements, which results unaffordable for most of machines and off-the-shelf solvers. Moreover, long-term inflation and degradation rates cannot be easily included in (4). These issues are solved in the following Section.

4. Solution via decomposition

4.1. Foundation

To better illustrate the solution strategy proposed, let us write (4) in a more compact form, as follows:

$$\min_{\substack{\overline{p}_z,\overline{H}_z,\delta_z,\boldsymbol{x}_{y,s},\boldsymbol{u}_{y,s},\\ \rho_{z,y,s,t},\lambda_{y,s},\mu_{y,s}}} \sum_{z\in Z}\sum_{y\in Y}\left\{f_y(\overline{p}_z,\overline{H}_z)+\omega_s\sum_{s\in S}g_{y,s}(\boldsymbol{x}_{y,s})\right\} \tag{5a}$$

Subject to:

$$(4b)-(4e) \tag{5b}$$

$$(2b)-(2t) \tag{5c}$$

$$(3) \tag{5d}$$

As seen, (5a) has a clear decomposable structure, encompassing planning costs that uniquely depend on planning decisions (i.e. $\overline{p}_z$ and $\overline{H}_z$) and operating costs which depend on day-ahead decision variables $\boldsymbol{x}_{y,s}$. This particular structure advocates to apply decomposition strategies in order to alleviate its intrinsic computational burden.

There is a variety of different decomposition techniques (see [46]). Among them, the Benders' decomposition is undoubtedly one of the most popular, finding multiple application in planning of power systems [39,47]. Subsequent sections detail the application of the Benders' decomposition to (5).

4.2. Overall procedure

The Benders' decomposition proceeds iteratively exchanging information between two levels. At the upper level, the so-called master problem decides on the value of planning variables (i.e. $\overline{p}_z$ and $\overline{H}_z$), while at the lower level, the subproblems determine operating decisions for given values of planning variables coming from the upper level. In the subproblems, sensitivities of planning decisions with respect to the function g in (5a) are derived in order to approximate this function at the master problem. The problem is iteratively repeated until a well-suited convergence criterion is met. Fig. 5 sketches the procedure of the Benders' decomposition approach.

4.3. Subproblems

A different subproblem is solved for each year and representative scenario. Each one solves the day-ahead hydrogen dispatch of the RS with the objective of maximizing its profit, thus resulting in the following optimization framework:

$$Profit^{\kappa}_{y,s}=\min_{\overline{p}_z,\overline{H}_z,p_{z,y,s,t},\atop \rho_{z,y,s,t}}\sum_{t\in T}\left\{\lambda^P_{z,y,s,t}p_{z,y,s,t}-L_y^{EV}h^{EV}_{z,y,s,t}\right\} \tag{6a}$$

Subject to:

$$(2q) \tag{6b}$$

$$(3a)-(3g) \tag{6c}$$

$$\overline{p}_z=\overline{p}_z^{\kappa}:\gamma_z^{\kappa};\forall z\in Z \tag{6d}$$

$$\overline{H}_z=\overline{H}_z^{\kappa}:\xi_z^{\kappa};\forall z\in Z \tag{6e}$$

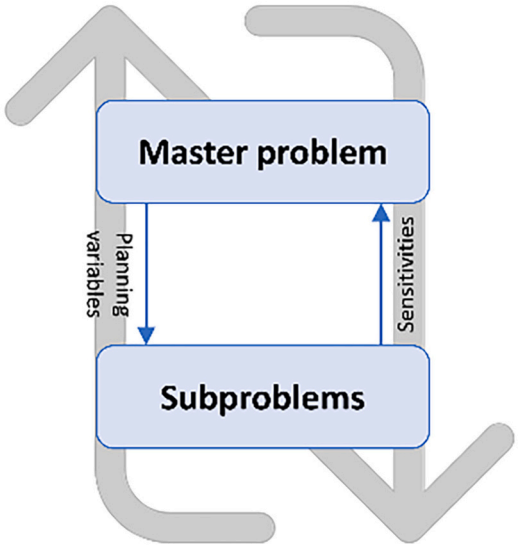

Fig. 5. Overall procedure of the Benders' decomposition approach.

For simplicity, iteration counters are only labelled on those variables that are exchanged between levels (the planning variables in this case). The objective (6a) calculates the profit of the RS at the y^{th} year and s^{th} scenario. (6b) bounds the electrolyser power and (6c) includes the rest of constraints pertaining to the RS model. Lastly, (6d) and (6e) fix the electrolyser and storage sizes to values coming from the master problem, allowing to derive the sensitivities γ and ξ, respectively.

The objective function (6a) determines that the RS pays under LMPs, which are determined as a by-product of the day-ahead dispatch of the DN. In the following section we detail how derive such prices in order to be included in (6).

4.4. Obtaining LMPs

LMPs can be derived as the dual variables of (2d). Nonetheless, as mentioned before, such dual variables cannot be derived directly from (2). To circumvent this issue, we firstly solve (2) to determine the electrolyser dispatching as well as the value of binary variables, as follows:

$$\widehat{\boldsymbol{u}}_{y,s}, \widehat{p}_{z,y,s,t} \in \underset{\substack{\boldsymbol{x}_s, \boldsymbol{u}_s, \rho_{z,y,s,t}, \\ \lambda_{y,s}, \mu_{y,s}}}{\operatorname{argmin}} NC\left(\overline{p}_z^{\kappa}\right) \tag{7a}$$

Subject to:

$$(2b) - (2t) \tag{7b}$$

$$(3) \tag{7c}$$

It is worth observing that the virtual RS agent has been included in (7c) and therefore (7) neglects the trivial solution $p_z = 0; \forall t \in T$. Once the value of $\widehat{\boldsymbol{u}}_{y,s}$ and $\widehat{p}_{z,y,s,t}$ have been obtained, the following linear counterpart of (7) can be solved:

$$\lambda^{P}_{z,y,s,t} \in \underset{\boldsymbol{x}_s}{\operatorname{argmin}} NC\left(\overline{p}_z^{\kappa}\right) \tag{8a}$$

Subject to:

$$p_{z,y,s,t} = \widehat{p}_{z,y,s,t}; \forall z \in Z \wedge t \in T \tag{8b}$$

$$(2b) - (2t) \tag{8c}$$

By fixing the electrolyser dispatch and binary variables, (7) and (8) result equivalent and therefore LMPs can be easily derived from (8) and used for solving (6).

4.5. Master problem

The master problem for the considered planning problem reads as

$$\overline{p}_z^{\kappa}, \overline{H}_z^{\kappa} \in \underset{\overline{p}_z^{\kappa}, \overline{H}_z^{\kappa}, \delta_z^{\kappa}, \beta_{y,s}^{\kappa}}{\operatorname{argmin}} \sum_{z \in Z} \left\{ \begin{array}{c} 1.2\overline{p}_z \left(K^Z + \sum_{y \in Y} O_y^Z \right) + 1.2\overline{H}_z \left(K^H + \sum_{y \in Y} O_y^H \right) + \\ \sum_{y \in Y} \omega_s \sum_{s \in S} \beta_{y,s}^{\kappa} \end{array} \right\} \tag{9a}$$

Subject to:

$$(4b) - (4d) \tag{9b}$$

$$\beta_{y,s}^{\kappa} \geq -M; \forall y \in Y \wedge s \in S \tag{9c}$$

$$\beta_{y,s}^{\kappa} \geq Profit_{y,s}^{\kappa} - \omega_s \left\{ \sum_{z \in Z} \left\{ \gamma_z^{\kappa} \left(\overline{p}_z^{\kappa} - \overline{p}_z^{\nu} \right) + \xi_z^{\kappa} \left(\overline{H}_z^{\kappa} - \overline{H}_z^{\nu} \right) \right\} \right\}; \forall y \in Y \wedge s \in S \wedge \nu \in \{1, 2, \ldots, \kappa - 1\} \tag{9d}$$

The objective (9a) is identical to (5a) but the function g is in this case approximated by the variable β, which is estimated using optimality cuts in (9d). In the rest of constraints, (9b) includes the planning constraints while (9c) avoid infeasibility at first iteration.

Note that $Y \times S \times (\kappa - 1)$ optimality cuts are included each iteration, thus resulting in a multi-cut strategy that eventually lead to a faster convergence [26]. Moreover, feasibility cuts [48] are not needed as the solution obtained after solving (9) is always feasible.

4.6. Further improvements

Below, we describe some modifications of the proposed Benders' decomposition algorithm to improve its convergence and properties.

Refining Master solutions: convergence of the Benders' decomposition can be accelerated in multiple ways [49]. One of them is improving the quality of the master solutions, i.e. the planning decision variables. In our case, electrolysers cannot import more power than the power limit of the corresponding node. Therefore, the following constraint can be included in (9) to avoid sub-optimal solutions:

$$\overline{p}_z^{\kappa} \leq \overline{F}_z; \forall z \in Z \tag{9e}$$

Regarding the storage tank, its capacity is also limited as

$$\overline{H}_z^{\kappa} \leq T \frac{\overline{p}_z^{\kappa} \eta^Z}{\mathrm{LHV}_{\mathrm{H_2}}}; \forall z \in Z \tag{9f}$$

As seen, the upper bound in (9f) corresponds to the hydrogen generated if the electrolyser works 24 h at rated power.

Valid sensitivities: sensitivities in (6) tend to be higher at those nodes where RSs are not installed. This behaviour is coherent since installing new electrolysers normally has a higher impact on the RS profit than increasing or decreasing the rated power of the already installed ones. This particular behaviour typically provokes oscillations of δ_z, which changes arbitrarily each iteration without stabilizing at a particular solution. To solve this issue, we propose to firstly consider that all the candidate buses have already installed a RS with the same electrolyser power. This way, the first iteration will provide the sensitivities of all nodes under the same conditions. Therefore, the second iteration will determine the most adequate bus/es for installing RS obeying to the highest sensitivities. After this iteration, the variable δ_z is fixed and the algorithm continues until convergence.

4.7. The algorithm

Below, we describe the step-by-step procedure for solving the considered planning problem using the Benders' decomposition approach.

Algorithm. Optimal sitting and sizing of refuelling stations via Benders' decomposition

Input: network data; scenarios (average and extreme) for electrical demands and renewable generators, wholesale market prices and hydrogen refuelling demand as well as their probability; parameters of distributed generators (dispatchable); capital and maintenance costs, expected lifetime and efficiency of electrolysers and hydrogen tanks; refuelling cost; inflation and degradation of parameters; lower-heating value of hydrogen; maximum number of stations and budget cap; parameters to linearize branch power flows (see Appendix).

Output: sizing and sitting of refuelling stations and expected profit.

Step 0: initialize $\kappa = 1$, $UB = \infty$, $LB = -\infty$, $\epsilon \in \Re_+$, $0 < \overline{p}_z^1 \leq \overline{F}_z$ and $\overline{H}_z^1 > 0$

Step 1: solve the master problem (9) and store $\beta_{y,s}^{\kappa}$, $\overline{p}_z^{\kappa}$ and $\overline{H}_z^{\kappa}$. If $\kappa = 1$, solve (9) without including (9b) and (9d). If $\kappa \geq 2$, take $\delta_z^{\kappa} = \delta_z^{\kappa-1}$. Else, store the value of δ_z^{κ}

Step 2: update $LB = \sum_{y \in Y} \omega_s \sum_{s \in S} \beta_{y,s}^{\kappa}$

Step 3: initialize $y = 1$

Step 4: update parameters according their inflation and degradation.

Step 5: initialize $s = 1$
Step 6: solve the problem (7) and update $\widehat{u}_{y,s}$ and $\widehat{p}_{z,y,s,t}$
Step 7: solve the problem (8) and update $\lambda^{P}_{z,y,s,t}$
Step 8: solve the problem (6) and store sensitivities γ^{κ}_{z} and ξ^{κ}_{z}
Step 9: update $s = s + 1$. If $s = S$ go to step 10. Else go to step 6.
Step 10: update $y = y + 1$. If $y = Y$ go to step 11. Else go to step 5.
Step 11: update $LB = \sum_{y \in Y} \omega_s \sum_{s \in S} Profit^{\kappa}_{y,s}$ and check convergence as

$$\frac{UB - LB}{UB} \leq \epsilon \tag{10}$$

where ϵ is the convergence threshold.
Step 12: if (10) holds then stop. Else, update $\kappa = \kappa + 1$ and go to step 1.

5. Numerical results

Throughout this Section we present and analyse a number of numerical results. The developed solution approach and optimization models were coded under Matlab R2021b and solved using Gurobi [50]. The Benders' algorithm is enforced to converge below $\epsilon = 0.05$.

5.1. Input data

Table 3 reports the data regarding electrolysers including costs and typical operating parameters of alkaline electrolysers. The lower-heating value of hydrogen was taken equal to 39.72 kWh/kg [40], while the degradation of electrolysers was considered 0.7%/year in line with the data reported in [51]. We consider that RSs are installed at the beginning of the project and dismantled at the end of the expected lifetime of electrolysers. The price of refilling hydrogen is 11 €/kg, according to some recent installations [52]. We consider an optimistic horizon in which the refilling cost is reduced progressively, in line with the conclusions in [53]. In this sense, we assume that hydrogen price is reduced by 2.6%/year and thus it takes a value of 7 €/kg at the end of the project lifetime. Table 4 shows the data regarding hydrogen storage, considering gaseous tanks. Maintenance costs are updated yearly taken an interest rate of 1.5% [54].

5.2. Network

We consider a modified IEEE radial 33-bus system as shown in Fig. 6, to which industrial and residential loads are connected together with renewable (wind and PV) and dispatchable generators, whose data are summarized in Table 5. For simplicity, we consider the same per-unit profiles for each kind of load or generator, which are based on real data from [60,61], and plotted in Fig. 7 together with their extreme scenarios constructed using the methodology described in Section 2.2. We consider a degradation of both PV panels and wind generators of 0.5%/year of their nominal power [31,62], while demand grows by 0.2%/year [63].

Price at substation corresponds with wholesale spot markets as shown in Fig. 8, which have been constructed according to market prices in Spain in 2018 [64] (discarding prices in the last three years significantly impacted by the COVID-19 pandemic and Ukraine's war). On the other hand, hydrogen demand is plotted in Fig. 8 and has been built up using the methodology described in [17]. This methodology considers probability distributions based on real-data. In particular, we consider the probability trip distribution reported in [65], which is based on real data and surveys. We therefore assume that the probability of a refilling event is directly related with the probability of daily trips, in line with [66]. On the other hand, the methodology considers assumes typical FCEV features for generating the hydrogen demand. In particular, a total hydrogen capacity of 5 kg and total range about 500–600 km. FCEV demand in Fig. 9 is generated assuming 20 refilling events per day and 10 dispensers per station, reasonable data taken into account the information in Fig. 1 and assuming that most of refilling events occur at morning and afternoon. We consider that both prices and FCEV demand grow by 1.5 and 0.2%/year, respectively. Finally, we consider that the exporting price (at substation) takes 0.7 times the importing one [32].

Table 3
Electrolyser data.

Parameter	Value	Ref.
Capital cost	400 €/kW	[55]
Maintenance cost	50 €/kW-year	[56]
Lifetime	15 years	[7]
Efficiency	73%	[57]

Table 4
Hydrogen storage data.

Parameter	Value	Ref.
Capital cost	305 €/kg	[58]
Maintenance cost	15 €/kg-year	[59]

5.3. Results

(a) LMPs

Fig. 10 plots the LMPs for the optimistic scenario. As seen, LMPs are notably low and frequently zero at nodes 12–18. This is due to the presence of two wind turbines near to these nodes, which allow them to be fully supplied through renewable sources. For the rest of nodes, LMPs mostly follow the wholesale electricity prices, indicating that the DN needs to import power to satisfy the local demand. In this regard, it is worth noting that local dispatchable generators are not scheduled at the optimistic scenario due to their marginal costs are higher than the price at the substation. However, these assets help to reduce LMPs in other scenarios as well as reducing the energy imported from the transmission system.

(b) Sitting and Sizing Results

Next, we analyse the main result of the developed panning tool, i.e. the optimal sitting and sizing of RSs in the DN. Firstly, we compare the results obtained for various values of the parameter N and $\Pi = 600$ k€ in Table 6. As observed, with $N = 1$ and 2 the node 16 is not selected despite it presents the lowest LMP as seen in Fig. 10. This is due to the power is limited at 300 kW at this node and therefore resulting more profitable installing RSs at other nodes with higher power limit. Actually, it is worth noting that the electrolysers installed with $N = 1$ and 2 have always >300 kW of rated power, which is the power limit at node 16. With $N = 3$, the algorithm leverages low LMPs at node 16 installing a 300 kW electrolyser. In summary, the developed tool seeks for installing the maximum electrolysis power possible, showing that the installed power is the most determinant result, clearly impacting the total project cost, which is notably reduced with the value of N.

It is also worth noting that the total project cost was always lower than zero, indicating a net profit. This result demonstrates the profitability of RSs even in a context with decreasing refilling prices. Regarding the total storage capacity, it resulted a function of the electrolyser rated power normally, thus indicating that storage tanks are normally sized according to the maximum hydrogen production at each node.

In Table 7, we compare the results obtained with $N = 2$ and different budget caps. As seen in this case, the selected nodes change without following a clear logic. However, when one analyses the total installed power in each case, a clear strategy can be deduced. Indeed, the algorithm seeks for installing the maximum electrolysis power in each case, which is clearly reflected in the total project cost as discussed in Table 6.

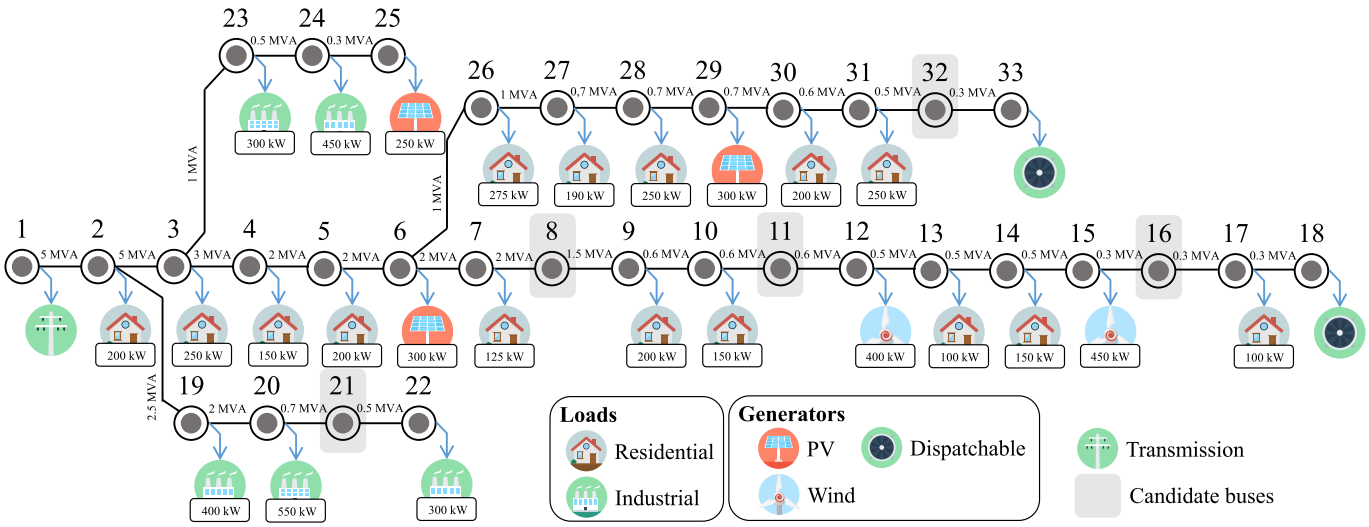

Fig. 6. The modified IEEE 33-bus system considered in simulations (power limits are shown on their corresponding branch).

Table 5
– Dispatchable generators data.

Parameter	Node	
	#18	#33
Rated power	400 kW	400 kW
Marginal cost	25 €/MWh	40 €/MWh
Minimum power	5% of its rated power	
Ramping limit	30% of its rated power	

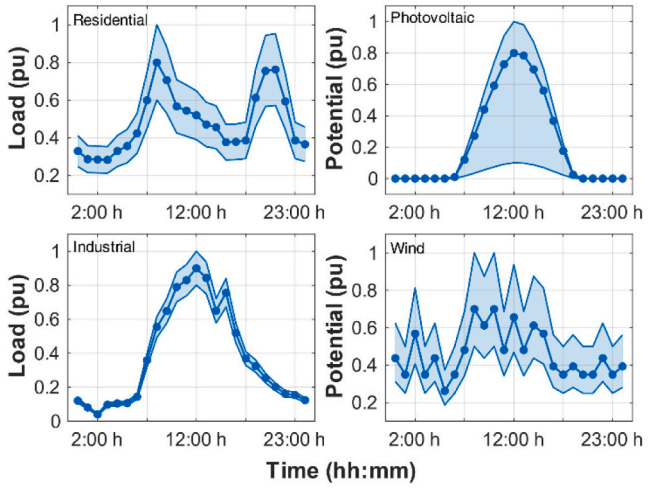

Fig. 7. Per unit profiles for demands and renewable generators.

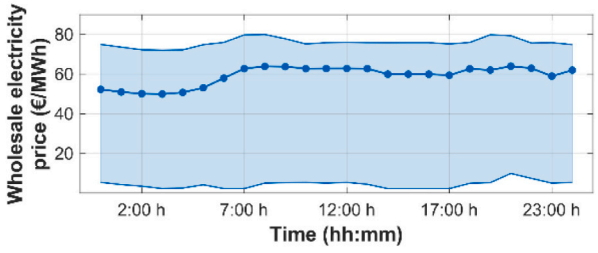

Fig. 8. Scenarios for wholesale electricity prices.

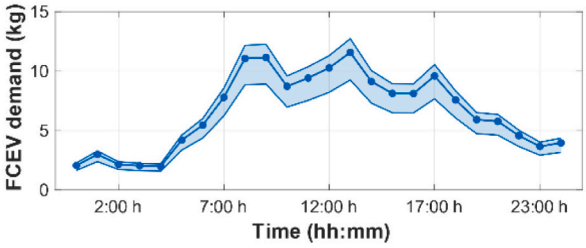

Fig. 9. Scenarios for FCEV refilling demand.

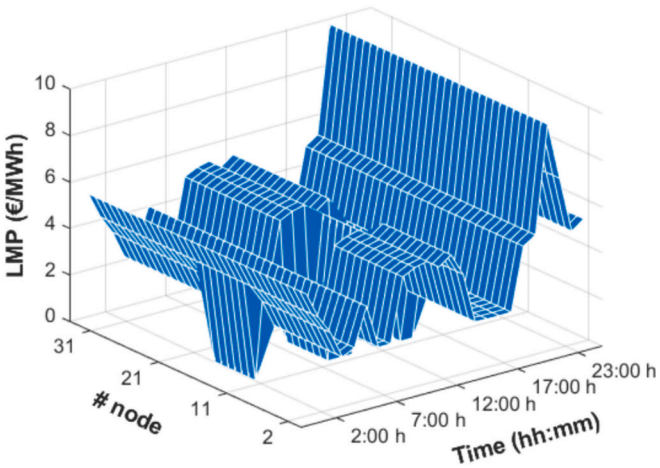

Fig. 10. Obtained LMPs for the optimistic scenario.

Table 6
Results obtained for different values of N and $\Pi = 600$ k€.

N	Node	$\overline{p}_z$ (net)	$\overline{H}_z$ (net)	Project cost (M€)
1	#8	415 kW	34 kg	−4.95
2	#21/#32	396/500 kW	49/71 kg	−9.27
3	#16/#21#32	300/435/430 kW	15/28/31 kg	−12.85
4	#8/#16/ #21#32	400/300/402/393 kW	23/15/23/26 kg	−16.80

Table 7
Results obtained for different values of Π and $N = 2$.

Π (k€)	Node	$\overline{p}_z$ (net)	$\overline{H}_z$ (net)	Project cost (M€)
150	#16/#21	157/153 kW	0/3.7 kg	−4.16
300	#8/#21	306/300 kW	14/13 kg	−7.37
450	#16/#21	300/443 kW	14/28 kg	−8.41
600	#16/#21	300/473 kW	13/33 kg	−8.41
750	#21/#32	396/500 kW	49/71 kg	−9.27

It is easy to see that the total installed power is higher as the available budget increases, thus remarking again that this result is the most significant for the economy of the project. This way, it is clear that results reported in Tables 6 and 7 are coherent, demonstrating that the developed tool follows the more logic strategy for increasing the profit of private investors.

In Table 7, one can see that increasing the budget above 450 k€ has a minor impact on the final project cost. This is due to installed electrolysis cannot be further increased due to power limits at nodes (note that the total power installed is barely increased from 743 to 900 kW). In the face of this situation, the developed tool tries to increase the profit by incrementing the storage capacity. However, this parameter has a limited impact on the monetary profit due to the low efficiency of electrolysers. Indeed, storage systems are profitable when differences in LMPs are sufficient to compensate the efficiency of the storage assets. Hence, in case of using electrolysers and hydrogen-based technologies, variation between peak and off-peak prices should be higher than for other storage technologies like batteries [22].

(c) Sensitivity Analysis

Fig. 11 compares the total project cost for different budget caps and number of RSs. As seen, both parameters contribute to improve the economy of investors by installing more electrolysis capacity and number of stations, respectively. In particular, the total project profit can be increased by 70% in case of installing more RSs and by 74% in case of increasing the budget, thus demonstrating that both parameters contribute notably to improve the economy of the project.

It is worth noting that the project cost cannot be further reduced above Π = 450 k€ in case of installing only one RS. This is due to project cost is mainly affected by the total power installed, as discussed before. In case of only installing one RS, its maximum electrolysis capacity is installed with Π = 450 k€ and therefore minor project reduction beyond that cap is only achieved by increasing the storage capacity, which has a less notable impact. One can see in Fig. 11 that similar conclusions can be drawn with $N = 2$ and 3 for particular budget caps in each case.

On the other hand, Fig. 12 shows the total hydrogen refilled throughout the project lifetime. One can check that results in Figs. 11 and 12 follow opposite trends, thus demonstrating that the final project cost is mainly ruled by the incomes from hydrogen refilling. This result explains why LMPs do not determine the RS location, as we mentioned previously, since costs from importing electricity have a marginal impact on the project profit.

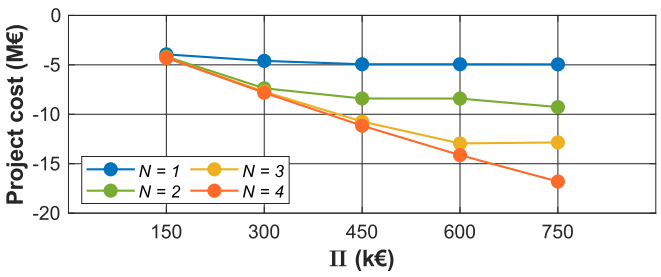

Fig. 11. Total project cost for different number of RSs and budget caps.

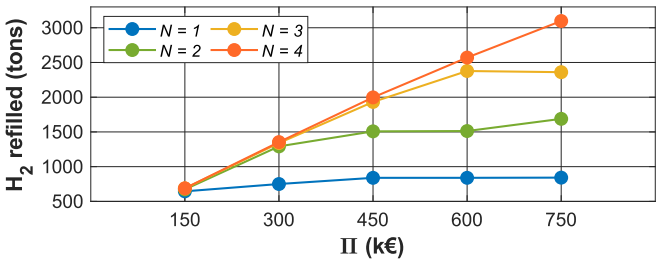

Fig. 12. Total hydrogen refilled for different number of RSs and budget caps.

(d) Electrolyser scheduling

Fig. 13 plots the scheduling plan for the electrolyser under the optimistic scenario, $N = 1$ and Π = 600 k€. As seen, the electrolyser is operated continuously during all the day and frequently close to its nominal power (~414.5 kW). More results are not included for simplicity but similar scheduling routine was observed in almost all the results obtained, which confirms that the simplified electrolyser modelling adopted in this paper is perfectly assumable and does not introduce notable inaccuracies in the project results.

Fig. 13 also shows the total hydrogen stored for this particular case. Not surprisingly, hydrogen tanks are filled at night. During these hours, low LMPs (see Fig. 10) are leveraged to produce a surplus hydrogen that is partially sent to hydrogen tanks. The hydrogen storage is fully filled at 7:00 h, when LMPs start growing. Then, hydrogen tanks are progressively emptied to refill FCEVs, thus complementing the operation of electrolysers. This particular behaviour reducing the total project cost by reducing the energy consumption of electrolysers notably. Moreover, deploying hydrogen storage allows reducing the size of electrolysers, which should be oversized to attend the full demand during afternoon. In this sense, part of the hydrogen stored during night when FCEV demand is low, can be used at afternoon, thus avoiding to supply all the demand from the electrolyser. Note that this is a typical behaviour of storage assets enabling energy arbitrage [22].

(e) Algorithm performance

Finally, we analyse the computational performance of the developed solution algorithm. To this end, the developed tool was run on an Intel (R) Core(TM) i7-8750H with 16 GB RAM personal laptop. Fig. 14 plots the total number of iterations required to converge for different number of RSs and budget caps. As seen, increasing the value of these two parameters leads to slow convergence. This is due to such settings expand the feasible space of the Master problem, which provides low quality solutions that cannot be properly approached through optimality cuts and sensitivities coming from subproblems. Note that this conclusion aligns with the recommendations in [49], where a number of accelerating strategies for the Benders' decomposition are based on improving the quality of the solution provided by the Master problem. Nevertheless, the algorithm is quite efficient even when many iterations are

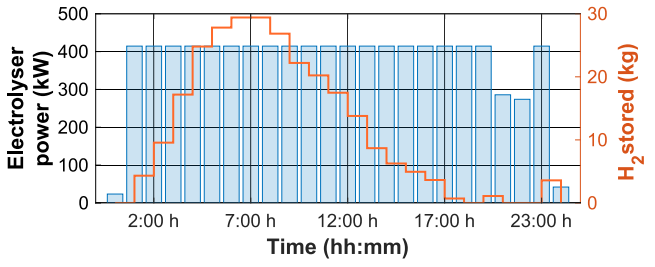

Fig. 13. Scheduling result for the electrolyser under the optimistic scenario, $N = 1$ and Π = 600 k€

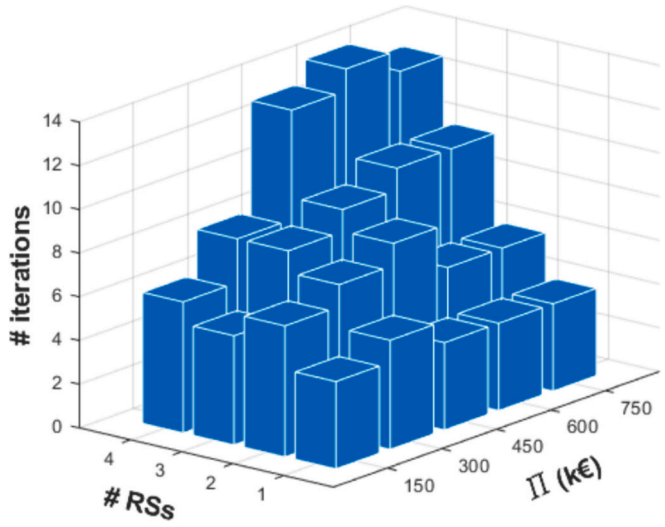

Fig. 14. Total number of iterations for different number of RSs and budget caps.

required, as shown in Fig. 15 where one can see that the total computational time is below 500 s and typically near to 200 s in all simulations, resulting perfectly assumable for planning tools.

5.4. Practical implications

The developed tool mainly serve for support-decision of DSO or RS investors, who need to decide optimally the sitting and sizing of their assets in order to maximize the expected profit. In this sense, the developed tool expects to find applications in any distribution system hosting RSs. This kind of application is expected to be valuable for countries where refilling infrastructure is expected to grow in the following years, such as China.

The developed planning methodology encrypts a day-ahead scheduling tool under LMPs for DNs including RSs. In this sense, the new proposal could be employed for DSOs to determine the scheduling plan of local assets and clear LMPs under the umbrella of distribution market arrangements.

Finally, it is worth mentioning that the developed tool serves to promote policies to incentivize the use and development of FCEVs in some countries where the use of this technology is marginal compared to battery vehicles, like Spain or other many European countries [2].

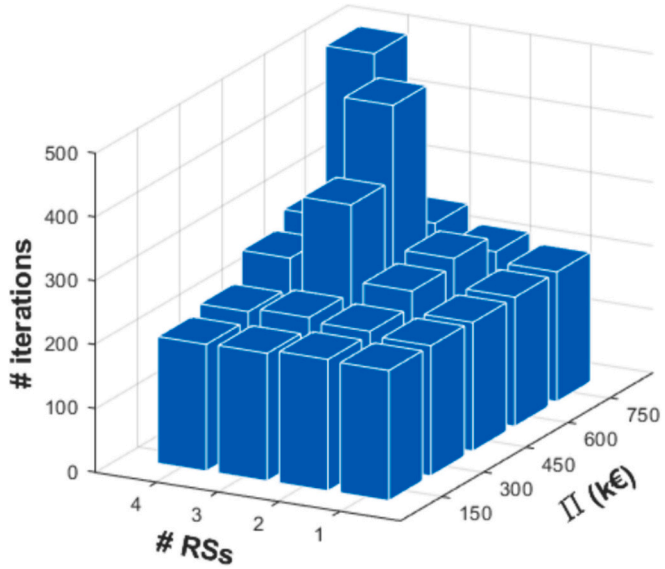

Fig. 15. Total computational time for different number of RSs and budget caps.

6. Conclusions and future works

A new optimal sitting and sizing tool for RSs in DNs has been developed. The new proposal strived for RSs with onsite storage and hydrogen generation through electrolysis. The developed methodology considers the influence of LMPs, which send proper signals for best allocate assets through the network. Finally, a multi-year iterative procedure based on the multi-cut Benders' algorithm has been proposed to alleviate the intrinsic high computational cost of the planning framework.

A number of simulations has been conducted in the well-known IEEE 33-bus system, encompassing renewable and dispatchable generators as well as residential and industrial loads. Results verified that LMPs effectively translate the real energy cost per node, thus serving to best sitting RSs in the network. This way, LMPs provide a valid signal to guide the scheduling plan for storage assets, which typically charge during night, when LMPs are low, and discharge at evening thus avoiding to import power during peak hours.

However, the power limit of each node turned out to be the most significant parameter for sitting stations. This result highlights the importance of upgrading electricity infrastructures when considering the installation of electrolysis facilities in existing power networks, which occasionally require to import much energy to produce sufficient hydrogen to attend the local refilling demand.

On the other hand, it has been highlighted that the installed electrolysis capacity reduces the cost of the project further. In this sense, it has been illustrated how the developed algorithm typically looks for the station configuration that maximizes that power. The impact of the budget cap and number of stations has been also discussed, showing that both parameters have similar influence on final results, reducing the total project cost by, approximately, 70%.

Finally, the computational performance of the developed algorithm has been analysed, thus demonstrating that the proposed framework is efficient and can be implemented in average machines.

To implement the developed tool, some prior data are needed. Most of the necessary data are normally available for DSOs without difficulty. Thus, expected local demand or renewable potential are normally measured and available in datasets. Moreover, many public datasets allow accessing to this kind of data in multiple geographical areas, which eases the implementation of the developed methodology. However, hydrogen refilling demand may be not publicly available. In this work, we have considered the methodology in [17], which is based on real-data from [63], to build up valid hydrogen demand profiles. Nevertheless, this is not a critical point for implementing the new proposal as it is more focused on planning stages, when considered input data can be estimated rather than measured [42].

Future works should be focused on developing novel energy management strategies for RSs encompassing electrolysers and storage, as well as discussing advanced bidding/offering strategies of such assets in energy and balance markets.

CRediT authorship contribution statement

Marcos Tostado-Véliz: Visualization, Validation, Supervision, Software, Resources, Project administration, Methodology, Conceptualization, Data curation, Formal analysis, Funding acquisition, Investigation, Writing – original draft, Writing – review & editing. **Pablo Horrillo-Quintero:** Writing – original draft, Visualization, Validation, Resources, Methodology, Conceptualization, Formal analysis, Writing – review & editing. **Pablo García-Triviño:** Validation, Supervision, Resources, Methodology, Investigation, Data curation, Formal analysis, Writing – review & editing. **Luis M. Fernández-Ramírez:** Project administration, Funding acquisition, Conceptualization, Data curation,

Supervision, Visualization. **Francisco Jurado:** Funding acquisition, Formal analysis, Data curation, Project administration, Supervision, Visualization, Writing – review & editing.

Declaration of competing interest

The authors declare that they have no known competing financial interests or personal relationships that could have appeared to influence the work reported in this paper.

Data availability

Data will be made available on request.

Acknowledgments

This work was partially supported by Ministerio de Ciencia e Innovación, Agencia Estatal de Investigación, and Unión Europea (Grants TED2021-129631B-C32 and TED2021-129631B-C31 supported by MCIN/AEI/10.13039/501100011033 and NextGenerationEU/PRTR).

Appendix A. Appendix

To linearize power flow limits in (2l), we employ the methodology described in [67]. Let us consider the following Euclidean norm constraint:

$$\underbrace{\sqrt{a^2+b^2}}_{\vartheta} \leq \overline{\vartheta} \tag{A1}$$

where a and b are variables and the square root term has been replaced by the dummy variable ϑ. Then, ϑ can be approximated by a set of intersecting planes $i \in \mathbb{I}$ described by three noncolinear points given by:

$$A_i = sin(i\theta - \theta) - sin(i\theta); \forall i \in \mathbb{I} \tag{A2}$$

$$B_i = cos(i\theta) - cos(i\theta - \theta); \forall i \in \mathbb{I} \tag{A3}$$

$$C_i = cos(i\theta)sin(i\theta - \theta) - cos(i\theta - \theta)sin(i\theta); \forall i \in \mathbb{I} \tag{A4}$$

where $\theta = 2\pi/|\mathbb{I}|$. This way, one can obtain the intersecting planes ϑ_i, as follows:

$$\vartheta_i = (A_i a + B_i b)/C_i; \forall i \in \mathbb{I} \tag{A5}$$

Making use of (A5), the constraint (A1) can be replaced by a set of $|\mathbb{I}|$ constraints of the form:

$$\vartheta_i \leq \overline{\vartheta}; \forall i \in \mathbb{I} \tag{A6}$$

Note that the true value of ϑ can be recovered as $\max_i \vartheta_i$, thus ensuring that actually (A6) is equivalent to (A1) for a particular $i \in \mathbb{I}$. The quality of this approximation strongly depends on the size of $\mathbb{I}$. It is advisable to create the minimum number of planes to ensure that power flows through branches are properly approximated. In our experiments, we could verify that tuning $|\mathbb{I}| = 256$ typically keeps the error below 2%.

References

[1] IEA. Global EV Outlook 2023. Paris: IEA; 2023. Online, available at: https://www.iea.org/reports/global-ev-outlook-2023. [Accessed 9 April 2024].
[2] Samsun RC, Rex M. Deployment of fuel cell vehicles in road transport and the expansion of the hydrogen refueling station network: 2023 update. Energy & Environment Band; 2023. Online, available at: https://www.ieafuelcell.com/fileadmin/publications/2023/2023_Deployment_of_Fuel_Cell_Vehicles_and_Hydrogen_Refueling_Station.pdf. [Accessed 9 April 2024].
[3] Gasnam, neutral transport. Mapa de estaciones de gas natural e hidrógeno. Online, available at: https://gasnam.es/mapa-estaciones-gas-natural-hidrogeno/. [Accessed 9 April 2024].
[4] Berger R. Hydrogen transportation - the key to unlocking the clean hydrogen economy. Online, available at: https://www.rolandberger.com/publications/publication_pdf/roland_berger_hydrogen_transport.pdf. [Accessed 9 April 2024].
[5] Qiu X, et al. Dynamic parameter estimation of the alkaline electrolysis system combining Bayesian inference and adaptive polynomial surrogate models. Appl Energy 2023;348:121533. https://doi.org/10.1016/j.apenergy.2023.121533.
[6] Xiao W, Cheng Y, Lee W-J, Chen V, Charoensri S. Hydrogen filling station design for fuel cell vehicles. IEEE Trans Ind Appl 2011;47(1):245–51. https://doi.org/10.1109/TIA.2010.2090934.
[7] Gökçek M, Kale C. Optimal design of a Hydrogen Refuelling Station (HRFS) powered by hybrid power system. Energy Convers Manag 2018;161:215–24. https://doi.org/10.1016/j.enconman.2018.02.007.
[8] Ayodele TR, Mosetlhe TC, Yusuff AA, Ntombela M. Optimal design of wind-powered hydrogen refuelling station for some selected cities of South Africa. Int J Hydrog Energy 2021;46(49):24919–30. https://doi.org/10.1016/j.ijhydene.2021.05.059.
[9] Gökçek M, et al. Optimum sizing of hybrid renewable power systems for on-site hydrogen refuelling stations: case studies from Türkiye and Spain. Int J Hydrog Energy 2024;59:715–29. https://doi.org/10.1016/j.ijhydene.2024.02.068.
[10] Grüger F, Dylewski L, Robinius M, Stolten D. Carsharing with fuel cell vehicles: sizing hydrogen refueling stations based on refueling behavior. Appl Energy 2018;228:1540–9. https://doi.org/10.1016/j.apenergy.2018.07.014.
[11] García-Triviño P, Torreglosa JP, Jurado F, Ramírez LMF. Optimised operation of power sources of a PV/battery/hydrogen-powered hybrid charging station for electric and fuel cell vehicles. IET Renew Power Gener 2019;13(16):3022–32. https://doi.org/10.1049/iet-rpg.2019.0766.
[12] Garcia-Torres F, Vilaplana DG, Bordons C, Roncero-Sánchez P, Ridao MA. Optimal management of microgrids with external agents including battery/fuel cell electric vehicles. IEEE Trans Smart Grid 2019;10(4):4299–308. https://doi.org/10.1109/TSG.2018.2856524.
[13] Tao Y, Qiu J, Lai S, Zhang X, Wang G. Collaborative planning for electricity distribution network and transportation system considering hydrogen fuel cell vehicles. IEEE Trans Transport Electrification 2020;6(3):1211–25. https://doi.org/10.1109/TTE.2020.2996755.
[14] Dadkhah A, Bozalakov D, De Kooning JDM, Vandevelde L. On the optimal planning of a hydrogen refuelling station participating in the electricity and balancing markets. Int J Hydrog Energy 2021;46(2):1488–500. https://doi.org/10.1016/j.ijhydene.2020.10.130.
[15] Lakouraj MM, Niaz H, Liu JJ, Siano P, Anvari-Moghaddam A. Optimal risk-constrained stochastic scheduling of microgrids with hydrogen vehicles in real-time and day-ahead markets. J Clean Prod 2021;318:128452. https://doi.org/10.1016/j.jclepro.2021.128452.
[16] Tabandeh A, Hossain MJ, Li L. Integrated multi-stage and multi-zone distribution network expansion planning with renewable energy sources and hydrogen refuelling stations for fuel cell vehicles. Appl Energy 2022;319:119242. https://doi.org/10.1016/j.apenergy.2022.119242.
[17] Tostado-Véliz M, Ghadimi AA, Miveh MR, Bayat M, Jurado F. Uncertainty-aware energy management strategies for PV-assisted refuelling stations with onsite hydrogen generation. J Clean Prod 2022;365:132869. https://doi.org/10.1016/j.jclepro.2022.132869.
[18] Abdelghany MB, Shehzad MF, Mariani V, Liuzza D, Glielmo L. Two-stage model predictive control for a hydrogen-based storage system paired to a wind farm

towards green hydrogen production for fuel cell electric vehicles. Int J Hydrog Energy 2022;47(75):32202–22. https://doi.org/10.1016/j.ijhydene.2022.07.136.
[19] Dong W, Shao C, Li X, Zhu D, Zhou Q, Wang X. Integrated planning method of green hydrogen supply chain for hydrogen fuel cell vehicles. Int J Hydrog Energy 2023;48(48):18385–97. https://doi.org/10.1016/j.ijhydene.2023.01.272.
[20] Tao Y, Qiu J, Lai S, Sun X. Coordinated planning of electricity and hydrogen networks with hydrogen supply chain for fuel cell electric vehicles. IEEE Trans Sustain Energy 2023;14(2):1010–23. https://doi.org/10.1109/TSTE.2022.3232596.
[21] Cardona P, et al. Modelling and operation strategy approaches for on-site hydrogen Refuelling stations. Int J Hydrog Energy 2024;52(B):49–64. https://doi.org/10.1016/j.ijhydene.2023.08.192.
[22] Wang X, Li F, Zhang Q, Shi Q, Wang J. Profit-oriented BESS siting and sizing in deregulated distribution systems. IEEE Trans Smart Grid 2023;14(2):1528–40. https://doi.org/10.1109/TSG.2022.3150768.
[23] Sun G, Li G, Li P, Xia S, Zhu Z, Shahidehpour M. Coordinated operation of hydrogen-integrated urban transportation and power distribution networks considering fuel cell electric vehicles. IEEE Trans Ind Appl 2022;58(2):2652–65. https://doi.org/10.1109/TIA.2021.3109866.
[24] Mo Y, Qin Z, Guo Y, Zhang Y. Day-ahead flexibility enhancement via joint optimization for new energy vehicle fleets and electric vehicle charging/hydrogen refuelling stations. IET Renew Power Gener 2022;16(12):2644–57. https://doi.org/10.1049/rpg2.12457.
[25] Conejo AJ, Castillo E, Minguez R, García-Bertrand R. Decomposition techniques in mathematical programming: Engineering and science applications. Berlin, Germany: Springer; 2006.
[26] Maldonado JL, Tostado-Véliz M, Hasanien HM, Khosravi N, Jurado F. Optimal planning of collective photovoltaic arrays in energy communities through a multi-cut benders' decomposition strategy. Sustain Cities Soc 2024;104:105307. https://doi.org/10.1016/j.scs.2024.105307.
[27] International Energy Agency. Electrolysers. Online, available at: https://www.iea.org/energy-system/low-emission-fuels/electrolysers. [Accessed 9 April 2024].
[28] Quincy Compressor. Full guide to air compressor safety. Online, available at: https://www.quincycompressor.com/tips-for-working-safely-with-compressed-air/. [Accessed 9 April 2024].
[29] Tostado-Véliz M, Hasanien HM, Jordehi AR, Turky RA, Jurado F. Risk-averse optimal participation of a DR-intensive microgrid in competitive clusters considering response fatigue. Appl Energy 2023;339:120960. https://doi.org/10.1016/j.apenergy.2023.120960.
[30] Tostado-Véliz M, Hasanien HM, Jordehi AR, Turky RA, Gómez-González M, Jurado F. An interval-based privacy – aware optimization framework for electricity price setting in isolated microgrid clusters. Appl Energy 2023;340:121041. https://doi.org/10.1016/j.apenergy.2023.121041.
[31] Mohamed AAR, Best RJ, Liu X, Morrow DJ. A comprehensive robust techno-economic analysis and sizing tool for the small-scale PV and BESS. IEEE Transa Energy Convers 2022;37(1):560–72. https://doi.org/10.1109/TEC.2021.3107103.
[32] Javadi MS, Lotfi M, Nezhad AE, Anvari-Moghaddam A, Guerrero JM, Catalão JPS. Optimal operation of energy hubs considering uncertainties and different time resolutions. IEEE Trans Ind Appl 2020;56(5):5543–52. https://doi.org/10.1109/TIA.2020.3000707.
[33] Blázquez J, Fuentes-Bracamontes R, Bollino CA, Nezamuddin N. The renewable energy policy paradox. Renew Sust Energ Rev 2018;82(1):1–5. https://doi.org/10.1016/j.rser.2017.09.002.
[34] Tostado-Véliz M, Liang Y, Jordehi AR, Mansouri SA, Jurado F. An interval-based bi-level day-ahead scheduling strategy for active distribution networks in the presence of energy communities. Sustain Energy, Grids Networks 2023;35:101088. https://doi.org/10.1016/j.segan.2023.101088.
[35] Al-Mubarak MJ, Conejo AJ. Storing freshwater versus storing electricity in power systems with high freshwater electric demand. J Mod Power Syst Clean Energy 2024;12(2):323–33. https://doi.org/10.35833/MPCE.2023.000306.
[36] Rooks C, et al. Robust hierarchical dispatch for residential distribution network management considering home thermal flexibility and model predictive control. IET Gener Transm Distrib 2021;15(18):2567–81. https://doi.org/10.1049/gtd2.12199.
[37] Gastalver-Rubio A, Romero-Ramos E, Maza-Ortega JM. Improving the performance of low voltage networks by an optimized unbalance operation of three-phase distributed generators. IEEE Access 2019;7:177504–16. https://doi.org/10.1109/ACCESS.2019.2958206.
[38] Raheli E, Werner Y, Kazempour J. A conic model for electrolyzer scheduling. Comput Chem Eng 2023;179:108450. https://doi.org/10.1016/j.compchemeng.2023.108450.
[39] Kazempour SJ, Conejo AJ. Strategic generation investment under uncertainty via benders decomposition. IEEE Trans Power Syst 2012;27(1):424–32. https://doi.org/10.1109/TPWRS.2011.2159251.
[40] Tostado-Véliz M, Kamel S, Hasanien HM, Turky RA, Jurado F. A mixed-integer-linear-logical programming interval-based model for optimal scheduling of isolated microgrids with green hydrogen-based storage considering demand response. J Energy Storage 2022;48:104028. https://doi.org/10.1016/j.est.2022.104028.
[41] Baumhof MT, Raheli E, Johnsen AG, Kazempour J. Optimization of Hybrid Power Plants: When is a Detailed Electrolyzer Model Necessary?. In: 2023 IEEE Belgrade PowerTech, Belgrade, Serbia; 2023. https://doi.org/10.1109/PowerTech55446.2023.10202860.
[42] Conejo AJ, Ruiz C. Complementarity, not optimization, is the language of markets. IEEE Open Access J Power Energy 2020;7:344–53. https://doi.org/10.1109/OAJPE.2020.3029134.
[43] Wang Y, et al. A Stackelberg game-based approach to transaction optimization for distributed integrated energy system. Energy 2023;283:128475. https://doi.org/10.1016/j.energy.2023.128475.
[44] Fortuny-Amat J, McCarl B. A representation and economic interpretation of a two-level programming problem. J Oper Res Soc 1981;32(9):783–92. https://doi.org/10.1057/jors.1981.156.
[45] Kleinert T, Schmidt M. Global optimization of multilevel electricity market models including network design and graph partitioning. Discret Optim 2019;33:43–69. https://doi.org/10.1016/j.disopt.2019.02.002.
[46] Conejo AJ, Castillo E, Minguez R, García-Bertrand R. Decomposition techniques in mathematical programming: Engineering and science applications. Berlin, Germany: Springer; 2006.
[47] Moreira A, Pozo D, Street A, Sauma E, Strbac G. Climate-aware generation and transmission expansion planning: a three-stage robust optimization approach. Eur J Oper Res 2021;295(3):1099–118. https://doi.org/10.1016/j.ejor.2021.03.035.
[48] Oliveira F, Grossmann IE, Hamacher S. Accelerating benders stochastic decomposition for the optimization under uncertainty of the petroleum product supply chain. Comput Oper Res 2014;49:47–58. https://doi.org/10.1016/j.cor.2014.03.021.
[49] Rahmaniani R, Crainic TG, Gendreau M, Rei W. The benders decomposition algorithm: a literature review. Eur J Oper Res 2017;259(3):801–17. https://doi.org/10.1016/j.ejor.2016.12.005.
[50] Gurobi Optimization L.L.C. Gurobi Optimizer Reference Manual. Online, available at: https://www.gurobi.com. [Accessed 10 April 2024].
[51] Horizon Europe. Increasing the lifetime of electrolyser stacks. Online, available at: https://www.horizon-europe.gouv.fr/increasing-lifetime-electrolyser-stacks-34825. [Accessed 10 April 2024].
[52] H2 live. H2 MOBILITY introduces dynamic pricing model as of 1st of October 23. Berlin, 1. Online, available at: https://h2.live/en/news/3126/. [Accessed 10 April 2024].
[53] Hydrogen Council. Path to Hydrogen Competitiveness. A Cost Perspective. Online, available at: https://hydrogencouncil.com/en/path-to-hydrogen-competitiveness-a-cost-perspective/. [Accessed 10 April 2024].
[54] Arévalo P, Tostado-Véliz M, Jurado F. A novel methodology for comprehensive planning of battery storage systems. J Energy Storage 2021;37:102456. https://doi.org/10.1016/j.est.2021.102456.
[55] International Energy Agency. Electrolysers. Online, available at: https://www.iea.org/energy-system/low-emission-fuels/electrolysers. [Accessed 10 April 2024].
[56] Christensen A. Assessment of Hydrogen Production Costs from Electrolysis: United States and Europe. The International Council on Clean Transportation; 2020. Online, available at: https://theicct.org/publication/assessment-of-hydrogen-production-costs-from-electrolysis-united-states-and-europe/. [Accessed 10 April 2024].
[57] Tostado-Véliz M, Jordehi AR, Fernández-Lobato L, Jurado F. Robust energy management in isolated microgrids with hydrogen storage and demand response. Appl Energy 2023;345:121319. https://doi.org/10.1016/j.apenergy.2023.121319.
[58] Clean Hydrogen Partnership. FCH 2 JU - MAWP Key Performance Indicators (KPIs). Online, available at: https://www.clean-hydrogen.europa.eu/knowledge-management/strategy-map-and-key-performance-indicators/fch-2-ju-mawp-key-performance-indicators-kpis_en. [Accessed 10 April 2024].
[59] Baghaee HR, Mirsalim M, Gharehpetian GB, Talebi HA. Reliability/cost-based multi-objective Pareto optimal design of stand-alone wind/PV/FC generation microgrid system. Energy 2016;115(1):1022–41. https://doi.org/10.1016/j.energy.2016.09.007.
[60] Carmona-Delgado C, Romero-Ramos E, Riquelme-Santos J. Fast and reliable distribution load and state estimator. Electr Power Syst Res 2013;101:110–24. https://doi.org/10.1016/j.epsr.2013.03.004.
[61] Engie Historical data reports Online, available at:. https://www.engieresources.com/historical-data#reports_anchor; n.d. [Accessed 28 May 2024].
[62] Staffell Iain, Green Richard. How does wind farm performance decline with age? Renew Energy 2014;66:775–86. https://doi.org/10.1016/j.renene.2013.10.041.
[63] International Energy Agency Electricity Consumption Online, available at:. https://www.iea.org/reports/electricity-information-overview/electricity-consumption; n.d. [Accessed 10 April 2024].
[64] Comisión Nacional de los Mercados y la Competencia. Precios Mercado. Online, available at: https://www.cnmc.es/estadistica/precios-mercado-2018. [Accessed 10 April 2024].
[65] Kurtz J, Sprik S, Saur G, Onorato S. Fuel cell electric vehicle driving and fueling behavior. National Renewable Energy Laboratory; 2019. NREL/TP-5400-73010.
[66] Negarestani S, Fotuhi-Firuzabad M, Rastegar M, Rajabi-Ghahnavieh A. Optimal sizing of storage system in a fast charging station for plug-in hybrid electric vehicles. IEEE Trans Transport Electrification 2016;2(4):443–53. https://doi.org/10.1109/TTE.2016.2559165.
[67] Giraldo JS, Vergara PP, López JC, Nguyen PH, Paterakis NG. A linear AC-OPF formulation for unbalanced distribution networks. IEEE Trans Ind Appl 2021;57(5):4462–72. https://doi.org/10.1109/TIA.2021.3085799.